

Jet directions in Seyfert galaxies: Radio continuum imaging data

H.R. Schmitt^{1,5}, J.S. Ulvestad², R.R.J. Antonucci³ and A.L. Kinney⁴

ABSTRACT

We present the results of VLA A-array 8.46 GHz continuum imaging of 55 Seyfert galaxies (19 Seyfert 1's and 36 Seyfert 2's). These galaxies are part of a larger sample of 88 Seyfert galaxies, selected from mostly isotropic properties, the flux at $60\mu\text{m}$ and warm infrared $25\mu\text{m}$ to $60\mu\text{m}$ colors. These images are used to study the structure of the radio continuum emission of these galaxies and their position angles, in the case of extended sources. These data, combined with information from broad-band B and I observations, have been used to study the orientation of radio jets relative to the plane of their host galaxies (Kinney et al. 2000).

Subject headings: galaxies:active – galaxies:jets – galaxies:Seyfert – galaxies:structure – galaxies:nuclei – radio continuum:galaxies

1. Introduction

Recently Schmitt et al. (1997), Clarke, Kinney & Pringle (1998) and Nagar & Wilson (1999) showed that there is little or no correlation between the position angle of radio jets and galaxy disk major axes in Seyfert galaxies. Employing a statistical inversion technique, which uses the observed values of δ (the difference between the position angle of the jet and the host galaxy disk major axis) and i (inclination of the galaxy disk relative to the line of sight), Clarke et al. (1998) and Nagar & Wilson (1999) showed that the observed δ -distribution can be reproduced by a homogeneous distribution of angles β (the angle between the jet and the galaxy disk axis).

¹Space Telescope Science Institute, 3700 San Martin Drive, Baltimore, MD 21218, USA

²National Radio Astronomy Observatory, P.O. Box 0, 1003 Lopezville Road, Socorro, NM87801

³University of California Santa Barbara, Physics Department, Santa Barbara, CA93106

⁴NASA Headquarters, 300 E St., Washington, DC20546

⁵email:schmitt@stsci.edu

These results confirm previous ones based on smaller samples (Ulvestad & Wilson 1984b; Brindle et al. 1990; Baum et al. 1993), and contradict the expectation that the jets should be aligned perpendicular to the galaxy disk. Assuming that the accretion disk and black hole are fed by gas from the host galaxy disk, it is natural to expect both disks to be aligned and have the same angular momentum vector. As a result, since jets are emitted perpendicular to the accretion disk, we would expect them to be aligned with the host galaxy minor axis, which is not observed. These studies give us information about the circumnuclear region of Seyferts and may be important in the study of processes involved in the feeding of the AGN. Possible explanations for the misalignment of the jet and the host galaxy disk are warping of the accretion disk, which can be caused by the self induced radiation instability (Pringle 1996; 1997; Maloney, Begelman & Pringle 1996), or by the misaligned inflow of gas from minor mergers (Barnes & Hernquist 1992, 1996). Kinney et al. (2000) give a complete list of possible causes of which we are aware for the observed misalignment.

The results from Clarke et al. (1998) and Nagar & Wilson (1999) were statistically significant. However, both papers were limited by the fact that they did not use well defined samples and most of their measurements were obtained from the literature. As a result, their results could suffer from selection effects, like the preferential selection of galaxies which have jets shining into the plane of the galaxy, resulting in brighter radio emission and narrow line regions, which would be easier to detect. The fact that these papers used data selected from the literature could also have influenced the results, because different authors are likely to measure the data using different techniques and use data of different quality.

In order to improve our analysis relative to previous studies, we obtained radio continuum images at 8.46 GHz (3.6cm), optical broad band images and spectroscopy for a sample of Seyfert galaxies selected from a mostly isotropic property, the flux at $60\mu\text{m}$, and warm infrared colors. In this way we avoid selection effects and create a homogeneous database, with measurements done using consistent techniques.

In this paper we present the VLA A-configuration X-band (8.46 GHz) observations of 55 of the Seyfert galaxies in our sample. The information about the remaining 20 galaxies for which there were data available in the literature is presented by Kinney et al. (2000) as are the statistical results of the position angle measurements. The broad-band B and I imaging data is presented by Schmitt & Kinney (2000). In Section 2 we present the sample. The description of the observations and reductions is given in Section 3, and the measurements are presented in Section 4. A summary is given in Section 5.

2. The Sample

As pointed out in the Introduction, previous works in this field probably suffered from selection effects, since they used samples obtained from the literature. In order to avoid these problems as much as possible, we have chosen a sample selected from a mostly isotropic property, the flux at $60\mu\text{m}$. Pier & Krolik (1992) models showed that the circumnuclear torus of Seyferts radiates nearly isotropically at $60\mu\text{m}$. Since these are the most anisotropic of the published models, they also are the most conservative.

We have chosen to use the de Grijp et al. (1987, 1992) and Keel et al. (1994) sample of warm IRAS galaxies, which were selected based on the quality of the $60\mu\text{m}$ flux measurements, Galactic latitude $|b| > 20^\circ$, and $25\mu\text{m}$ – $60\mu\text{m}$ color in the range $-1.5 < \alpha(25/60) < 0$. This color criteria excluded starburst galaxies as much as possible, but the galaxies were also observed spectroscopically to confirm their activity types (de Grijp et al. 1992). Our sample includes all the Seyferts in de Grijp et al. (1987, 1992) which had redshift $z \leq 0.031$, giving a total of 88 galaxies (29 Seyfert 1's and 59 Seyfert 2's). This distance limit is large enough to include a substantial number of galaxies to provide good statistics, but still close enough to allow the resolution of radio features. More details about the sample selection are given by Kinney et al. (2000).

Of the 88 galaxies in our sample, 77 have $\delta > -47^\circ$ and can be observed from the VLA. Here we present our observations of 36 of these galaxies, and images of 19 other galaxies for which data were extracted from the VLA archive. For 20 other galaxies we were able to obtain measurements from the literature, giving a total of 75 Seyfert galaxies with high resolution 8.46GHz (3.6cm) radio observations.

Table 1 presents the galaxies observed by us, and those for which we reduced VLA archival data. The measurements for the entire sample of 88 galaxies, including the galaxies for which we obtained radio observations from the literature, is presented by Kinney et al. (2000) and Schmitt & Kinney (2000). The Table gives the identification numbers of the galaxies in the de Grijp et al. (1987) catalog, their names, activity types, dates in which the observations were done, the codes of the VLA proposals from which the data were obtained, the observational method used to observe the sources (S) and the phase calibrators (C), the integrated 3.6cm flux densities, the $1-\sigma$ noise levels, the position angles of the extended radio structures (PA_{RAD}), the sizes of the radio sources (calculated assuming $H_0 = 75 \text{ km s}^{-1} \text{ Mpc}^{-1}$) their morphologies, and in the case of archival data, the reference where the data have already been published.

3. Observations and reductions

All the observations presented in this paper were obtained with the VLA in A-configuration at 8.46 GHz. Of the 55 galaxies presented here, 36 were observed by us (proposal AA226) and the other 19 were obtained from 7 other projects for which there were data available in the VLA archive. The dates in which the galaxies were observed and their respective VLA proposal codes are given in columns 4 and 5, respectively, of Table 1.

The observations were done in snapshot mode, using 3C286 and/or 3C48 as primary flux calibrators (depending on the proposal). Most of the observations were done using J2000.0 coordinates with the exception of 7 galaxies, observed by the projects AB618, AD244, AK350, AK407 and AP276, which were observed using B1950.0 coordinates and later converted to J2000.0 with AIPS. The phase calibration was done using calibrators from the NRAO list, preferentially using A-category calibrators closer than 10° from the galaxies. Most of the observations were done sandwiching \sim 10 minutes observations of the galaxy (S) with short \sim 2–3 minutes observations of a phase calibrator (C), repeating the process for 3 to 7 times, which gives a total on source integration time of 30 to 90 minutes. For 14 galaxies, observed in the proposals AK394 and AD244, the source was observed only once, for \sim 15 minutes, followed by a \sim 5 minute observation of the phase calibrator. The observing methods used for each galaxy are shown in the 6th column of Table 1, where “CSC...” means that the source was sandwiched with observations of the phase calibrator, and “CS” that the source and phase calibrator were observed only once.

The reductions were done using AIPS and following standard techniques. In the case of sources observed in the “CSC...” mode, the phase calibration was done by linearly interpolating between the observations of the phase calibrator, while for sources observed in the “CS” mode, the data was first boxcar smoothed and then interpolated. The images were made using uniform weighting, all the sources were interactively self-calibrated in phase and imaged.

Typical resolutions in our final images were $0.20'' - 0.25''$. Because the VLA A-configuration is not sensitive to structures with scale sizes larger than about $7''$ at 3.6 cm, the results reported here generally refer to small-scale properties of the galaxy nuclei, rather than global properties of the entire galaxies. In particular, for this reason, source sizes and position angles do not include emission from the galaxy disks.

4. Measurements

In Figure 1 we present the contour plots of the observed galaxies. Of the 55 galaxies observed, only TOL1238-364 was not detected. The total flux densities of the sources (Stokes parameter I) were measured integrating over the images, taking into account the background level, and are given in column 7 of Table 1. We also used the deconvolved images to determine the $1-\sigma$ noise level of the images. These values vary from $22 \mu\text{Jy}/\text{beam}$ to $109 \mu\text{Jy}/\text{beam}$, but typically are around $30 \mu\text{Jy}/\text{beam}$ to $60 \mu\text{Jy}/\text{beam}$. The smaller values correspond to the galaxies with the higher integration time, while the higher ones correspond to the galaxies with shorter integrations, or those observed through a high air mass. These values are given in column 8 of Table 1.

The radio images were decomposed by fitting gaussians to their individual components. The positions of these components and their respective fluxes are given in Table 2. Comparing the total fluxes obtained in this method with the fluxes measured directly from the images (Table 1) we find an agreement of 5% to 10% for most of the galaxies, especially the ones with unresolved emission. In the case of slightly resolved sources and sources with diffuse emission, the agreement is not always as good as 10%, since the gaussians tend to separate the compact emission only.

For those galaxies with extended radio emission, we present in column 9 of Table 1 the measured Position Angle of this emission (PA_{RAD}). These values were obtained from the positions of the individual gaussians fitted to the data, or, in the case of galaxies with more extended emission, measured directly on the images. These measurements have an uncertainty of $3 - 5^\circ$ for linear extended sources and $5 - 10^\circ$ for slightly resolved ones. The linear sizes of the radio sources, calculated assuming $H_o = 75 \text{ km s}^{-1} \text{ Mpc}^{-1}$, are given in column 10 of Table 1. Finally, the structure of the radio emission, classified according to the Ulvestad & Wilson (1984b) definition is given in column 11 of Table 1 (L=linear, D=diffuse, S=slightly extended, U=unresolved).

4.1. Flux Density and Position Measurement Errors

Errors involved in the flux density measurements are due to two different sources. The first and most important one is the uncertainty in transferring the amplitude scale of the primary flux calibrator, which is of the order of 5% at 8.46 GHz and dominates the errors. The second source of error is the noise in the images. These two values have to be added in quadrature, and the contribution from the noise in the images is important only for those galaxies where this value is similar to the one due to the amplitude scale of the calibrator,

usually objects with integrated fluxes smaller than 1.0 mJy.

We estimate that the errors in the positions of the individual components presented in Table 2 are of the order of 0.01-0.03'', in both Right Ascention and Declination. Several sources contribute to this error, and they have to be added in quadrature. The first one is the uncertainty in the positions of the phase calibrators. Most of the observations presented here were done with A-category calibrators, which have position uncertainties $< 0.002''$, so this error is negligible in most of the cases. The second source is the error in the gaussian fitting to the individual components, which we determine to be of the order of 0.005'' for the measurements presented here. A third source of error is due to the strength of the detected emission. For a detection with a given signal to noise ratio (S/N), the position of the source cannot be determined with an accuracy better than (beam size)/(S/N). The typical beamsize of our observations is 0.25'', so this source of error is dominant for components where the detection has $S/N \leq 10$.

4.2. Individual Objects

In this section we discuss the observed radio structures of the galaxies with extended emission.

4.2.1. *UGC2514*

This galaxy presents a nuclear point source and an extended source to the SW, along PA=56°. The total extent of the radio emission is 70 parsecs.

4.2.2. *IRAS03106-0254*

Norris et al. (1990) detected a compact nuclear source in this galaxy, with flux of 12 mJy at 2.3 GHz. Our radio image was decomposed into 3 components, extended along the NE-SW direction PA=37°. The radio source is extended by 850 parsecs.

4.2.3. *IRAS04502-0317*

Spectropolarimetric observations (Kay 1994) show that this galaxy presents a very small amount of polarization $\approx 0.5\%$ around 4400Å and the HST F606W image (Malkan,

Gorjian & Tam 1998) shows a dust lane crossing the nucleus. This galaxy has a weak double radio source, extended along PA=22°, with a dimension of 110 parsecs.

4.2.4. *IRAS04507+0358*

The stellar population synthesis of the nuclear spectrum of this galaxy shows that it is dominated by old stars, with a small ($\approx 5\%$) contribution from 100Myr stars (Schmitt, Storchi-Bergmann & Cid Fernandes 1999). The [OIII] $\lambda 5007\text{\AA}$ image shows halo like extended emission (Mulchaey, Wilson & Tsvetanov 1996). The radio emission of this galaxy is slightly resolved, having an extent of 210 parsecs along PA=153°.

4.2.5. *MRK6*

The radio image of this galaxy presents an intricate morphology, with a linear double structure along the N-S direction (PA= −3°) and a low surface density structure, similar to a ring, approximately perpendicular to the jet. This ring structure has been previously detected by Baum et al. (1993), Kukula et al. (1996) and Xu et al. (1997). Baum et al. (1993) also detected radio lobes extending up to 40'' from the nucleus. The jet is extended by 440 parsecs, while the ring like structure is extended by ~ 1800 parsecs. Neutral Hydrogen mapping of the nuclear region by Gallimore et al. (1999) shows HI absorption against the northern part of the jet, possible due to a dust lane crossing north of the nucleus. Kukula et al. (1996) compared MERLIN high resolution radio observations and [OIII] $\lambda 5007\text{\AA}$ images of this galaxy, showing that they are misaligned. They suggest that this misalignment is due in part to a projection effect, where the jet is emitted at an angle relative to the galaxy disk and the gas emission comes from ionized gas in the disk of the galaxy.

4.2.6. *MRK79*

Ulvestad & Wilson (1984a) detected extended radio emission at 6 cm and 20 cm in this galaxy. The 3.6cm radio image presented here confirms their results, an asymmetric triple radio structure along PA= 11°. The distance between the nucleus and the northern source is 800 parsecs, while that to the southern source is 460 parsecs. Nazarova, O'Brien & Ward (1996) detected extended line emission along PA= 12°, based on spectroscopic observations.

4.2.7. *MCG-01-24-012*

The radio emission of this galaxy is extended to the W (PA= 89°) by 130 parsecs.

4.2.8. *NGC3393*

The X-ray spectrum of this galaxy (Maiolino et al. 1998) has a hard flux $F_{2-10KeV} = 3.9 \times 10^{-13}$ erg cm $^{-2}$ s $^{-1}$, and can be fitted with a power law Compton thick absorbed spectrum ($N_H > 10^{25}$ cm $^{-2}$) reflected by cold gas in our direction. A detailed analysis of the ultraviolet spectrum of this galaxy can be found in Díaz, Prieto & Wamsteker (1988). The radio emission can be decomposed into 4 different components along the NE-SW direction, with total extent of 680 parsecs. The nucleus and the stronger components are along PA= 56°. The SW component shows some diffuse emission to the S, and the NE component shows a second component to the N. A comparison between the radio image and the HST [OIII] $\lambda 5007\text{\AA}$ emission (Schmitt & Kinney 1996), shows that the radio emission is encircled by the [OIII] emission, suggesting a shock front that ionizes the gas.

4.2.9. *IRAS11215-2806*

The nuclear stellar population of this galaxy (Schmitt et al. 1999) is dominated by old stars, with a small contribution ($\approx 5\%$) from 100Myr old stars. This galaxy shows several radio blobs. The strongest ones are extended by ~ 200 parsecs along PA= 75°, with a weaker source 400 parsecs to the SW of the nucleus (PA= 226°).

4.2.10. *MCG-05-27-013*

The nuclear stellar population of this galaxy (Schmitt et al. 1999) has contributions only from stars older than 1 Gyr. The HST F606W image (Malkan et al. 1998) shows a strong dust lane to the N of the nucleus. The overall radio emission of this galaxy is extended by 1530 parsecs along PA= 2°. It shows the nucleus, a detached blob to the N and a diffuse source to the S.

4.2.11. MRK176

This is an interacting Seyfert 2 galaxy. According to Veilleux, Goodrich & Hill (1997), it may have a broad $\text{Pa}\beta$ emission line. The radio emission is slightly extended by 140 parsecs along PA= 92°.

4.2.12. MCG-04-31-030

According to Pogge (1989) the [OIII] and $\text{H}\alpha$ images of this galaxy do not show extended emission. The hard X-ray spectrum can be fitted with a double power-law and has a flux $F_{2-10\text{ kev}}=3.56\times10^{-12}\text{ erg cm}^{-2}\text{ s}^{-1}$ (Turner et al. 1997). The HST F606W image (Malkan et al. 1998) shows a bright nuclear source and a dust lane to the N of the nucleus. This galaxy shows a low flux density linear structure extended by 480 parsecs along PA= 85°.

4.2.13. MCG-03-34-064

According to Roy et al. (1998), this galaxy has a compact nuclear radio source with a flux of 26 mJy at 2.3 GHz. The optical and ultraviolet spectra show narrow emission lines with blueward assymmetries and possibly a broad $\text{CIV}\lambda1550\text{\AA}$ line (De Robertis, Hutchings & Pitts 1988). The radio emission is extended by 280 parsecs. It starts as a linear structure to the SW (PA= 219°) and after \sim 100 parsecs it bends to the S, along PA≈ 180°. Kay (1994) spectropolarimetric data showed that the nuclear spectrum of this galaxy is polarized by 7.4% at 4400\AA , along PA= 109°, approximately perpendicular to the extended radio emission. We adopt the innermost PA as the direction of the jet.

4.2.14. ESO383-G18

This galaxy shows a slightly extended radio structure to the N of the nucleus (PA= -2°) extended by 110 parsecs.

4.2.15. *IRAS14082+1347*

The Malkan et al. (1998) HST F606W image of this galaxy shows a dust lane crossing to the north of the nucleus. The radio emission is slightly extended to the W, along PA= 279°, with a total extent of 55 parsecs.

4.2.16. *NGC5506*

According to Braatz, Wilson & Henkel (1996) this galaxy has an H₂O maser. The radio emission shows a linear structure along the E-W direction, surrounded by diffuse emission, with a total extension of 300 parsecs. The VLBA image from Roy et al. (2000) shows a double radio source along PA= 70°, which will be used by Kinney et al. (2000). This galaxy is almost edge-on and the HI image (Gallimore et al. 1999) shows absorption against the nuclear source. The hard X-ray spectrum has a flux $F_{2-10\text{Kev}} = 8.38 \times 10^{-11} \text{ erg cm}^{-2} \text{ s}^{-1}$ and is absorbed by a column density $N_H = 3.4 \times 10^{22} \text{ cm}^{-2}$ (Bassani et al. 1999). Maiolino et al. (1994) detected double peaked line profiles, which they interpreted as outflow along PA= -16°. Colbert et al. (1998) detected extended soft X-ray emission along the same direction, PA= -20°, which is also coincident with the extended radio emission.

4.2.17. *IRAS14317-3237*

This galaxy shows a radio structure extended by 290 parsec along PA= 169°.

4.2.18. *UGC9944*

The radio emission of this galaxy is a symmetric triple source with total extent of 3430 parsecs along PA= 67°. The SW component can be decomposed into 2 sources, separated by \approx 140 parsecs.

4.2.19. *AKN564*

According to Boller, Brandt & Fink (1996) this is an X-ray variable Narrow Line Seyfert 1 galaxy with a steep spectrum, photon index $\Gamma \approx 3$ in the range 0.1-2.4Kev. It has a triple radio source along the N-S direction (PA= 6°), extended by 320 parsecs. This is

consistent with the result shown by Moran (2000).

4.2.20. *MCG+8-11-11*

The first radio observations of this galaxy were done by Wilson & Willis (1981), using the VLA at 6cm, which showed a strong nuclear source and some extended emission in the N-S direction. Ulvestad & Wilson (1986) presented a VLA image at 2cm, showing a triple radio source, extended by $\approx 1''$ along PA= 127°. Our radio image at 3.6cm shows a central component extended along PA= 128°, surrounded by diffuse emission along the N-S direction, with a total extent of 1230 parsecs. This structure is similar to the one observed by Ulvestad & Wilson (1986) at 6cm. The HST [OIII] and H α images of this galaxy show no evidence of extended emission (Bower et al. 1994; Schmitt & Kinney 1996).

4.2.21. *NGC4941*

Maiolino et al. (1999) presented the X-ray spectrum of this galaxy, which has a soft band flux $F_{0.5-2Kev} = 2.08 \times 10^{-13}$ erg cm $^{-2}$ s $^{-1}$, a hard band flux $F_{2-10Kev} = 6.63 \times 10^{-13}$ erg cm $^{-2}$ s $^{-1}$, and can be fitted with a power law absorbed by a column density $N_H = 4.5 \times 10^{23}$ cm $^{-2}$. The [OIII] emission (Pogge 1989) has a halo like morphology and the H α image shows HII regions along the spiral arms. This is the smallest extended source in our sample, presenting a double radio source extended by 15 parsecs along PA= -25°. This source was only slightly resolved in previous radio observations (Ulvestad & Wilson 1989).

5. Summary

We presented VLA A-configuration observations of 55 Seyfert galaxies at 8.46GHz. These galaxies are part of a sample of 88 Seyfert galaxies selected from a mostly isotropic property, the flux at 60 μ m, and warm infrared colors. Only one of the 55 galaxies, TOL1238-364 was not detected, and 21 galaxies show extended emission. We measured the radio flux densities of these galaxies, the sizes of their emitting regions, the Position Angle of the extended radio emission (PA_{RAD}) and their morphologies. These measurements have been combined with information from broad-band B and I observations to study the orientation of radio jets relative to the host galaxy disk (Kinney et al. 2000).

We would like to thank Jim Pringle for useful discussions. HRS would like to

thank the hospitality of the NRAO staff in Socorro, where the data was reduced and analyzed. This work was supported by NASA grants NAGW-3757, AR-5810.01-94A, AR-6389.01-94A and the HST Director Discretionary fund D0001.82223. This research made use of the NASA/IPAC Extragalactic Database (NED), which is operated by the Jet Propulsion Laboratory, Caltech, under contract with NASA. The National Radio Astronomy Observatory is a facility of the National Science Foundation operated under cooperative agreement by Associated Universities, Inc.

REFERENCES

Barnes, J.E., & Hernquist, L., 1992. *ARA&A*, 30, 70

Barnes, J.E., & Hernquist, L. 1996. *ApJ*, 471, 115

Bassani, L., Dadina, M., Maiolino, R., Salvati, M., Risaliti, G., Della Ceca, R., Matt, G. & Zamorani, G. 1999, *ApJS*, 121, 473

Baum, S. A., O'Dea, C. P., Dallacassa, D., de Bruyn, A. G. & Pedlar, A. 1993, *ApJ*, 419, 553

Baum, S.A., O'Dea, C.P., de Bruyn, A.G., & Pedlar, A. 1993, *ApJ*, 419, 553

Boller, Th., Brandt, W. N. & Fink, H. 1996, *A&A*, 305, 53

Bower, G. A., Wilson, A. S., Mulchaey, J. S., Miley, G. K., Heckman, T. M. & Krolik, J. H. 1994, *AJ*, 107, 1686

Braatz, J. A., Wilson, A. S. & Henkel, C. 1996, *ApJS*, 106, 51

Brindle, C., Hough, J.H., Bailey, J.A., Axon, D.J., Ward, M.J., Sparks, W.B., & McLean, I.S. 1990, *MNRAS*, 244, 577

Clarke, C.J., Kinney, A.L., & Pringle, J.E. 1998, *ApJ*, 495, 189

Colbert, E. J. M., Baum, S. A., O'Dea, C. P. & Veilleux, S. 1998, *ApJ*, 496, 786

De Grijp, M.H.K., Keel, W. C., Miley, G.K., Goudfrooij, P. & Lub, J. 1992, *A&AS*, 96, 389

De Grijp, M.H.K., Miley, G.K., & Lub, J. 1987, *A&AS*, 70, 95

De Robertis, M. M., Hutchings, J. B. & Pitts, R. E. 1988, *AJ*, 95, 1371

Díaz, A. I., Prieto, M. A. & Wamsteker, W. 1988, *A&A*, 195, 53

Gallimore, J. F., Baum, S. A., O'Dea, C. P., Pedlar, A. & Brinks, E. 1999, *ApJ*, 524, 684

Kay, L. E. 1994, *ApJ*, 430, 196

Keel, W.C., de Grijp, M. H. K., Miley, G. K. & Zheng, W. 1994, *A&A*, 283, 791

Kinney, A.L., Schmitt, H.R., Clarke C.J., Pringle, J.E., Ulvestad, J.S., & Antonucci, R.R.J. 2000, *ApJ*, 537, 152

Kukula, M. J., Holloway, A. J., Pedlar, A., Meaburn, J., Lopez, J. A., Axon, D. J., Schilizzi, R. T. & Baum, S. A. 1996, *MNRAS*, 280, 1283

Maiolino, R., Salvati, M., Bassani, L., Dadina, M., Della Ceca, R., Matt, G., Risaliti, G. & Zamorani, G. 1998, *A&A*, 338, 781

Maiolino, R., Stanga, R., Salvati, M. & Rodríguez Espinosa, J. M. 1994, *A&A*, 290, 40

Malkan, M. A., Gorjian, V. & Tam, R. 1998, *ApJS*, 117, 25

Maloney, P.R., Begelman, M.C. & Pringle, J.E., 1996, *ApJ*, 472, 582

Moran, E. C. 2000, *New Astronomy*, in press

Mulchaey, J. S., Wilson, A. S. & Tsvetanov, Z. 1996, *ApJS*, 102, 309

Norris, R. P., Allen, D. A., Sramek, R. A., Kesteven, M. J. & Troup, E. R. 1990, *ApJ*, 359, 291

Nagar, N.M., & Wilson, A.S. 1999, *ApJ*, 516, 97

Nazarova, L. S., O'Brien, P. T. & Ward, M. J. 1996, *A&A*, 307, 365

Pier, E.A., & Krolik, J.H., 1992, *ApJ*, 401, 99

Pogge, R. W. 1989, *ApJ*, 345, 730

Pringle, J.E., 1996. *MNRAS*, 281, 357

Pringle, J.E., 1997. *MNRAS*, 292, 136

Roy, A.L. et al. 2000, in *Perspectives in Radio Astronomy: Imperatives at cm and m Wavelengths* (Dwingeloo: NFRA), Eds: M.P. van Haarlem & J.M. van der Hulst

Roy, A. L., Norris, R. P., Kesteven, M. J., Troup, E. R. & Reynolds, J. E. 1998, *MNRAS*, 301, 1019

Schmitt, H. R. & Kinney, A. L. 1996, *ApJ*, 463, 623

Schmitt, H.R. & Kinney, A.L. 2000, *ApJS*, in press

Schmitt, H.R., Kinney, A.L., Storchi-Bergman, T., & Antonucci, R. 1997, *ApJ*, 477, 623

Schmitt, H. R., Storchi-Bergmann, T. & Cid Fernandes, R. 1999, *MNRAS*, 303, 173

Thean, A., Pedlar, A. Kukula, M. J., Baum, S. A. & O'Dea, C. 2000, *MNRAS*, 314, 573

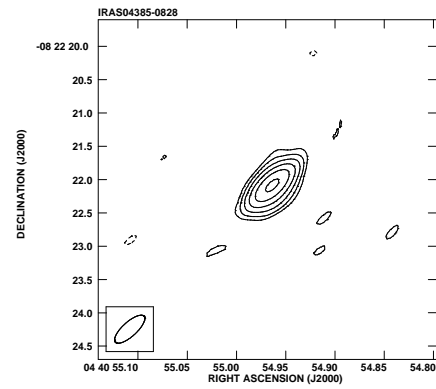
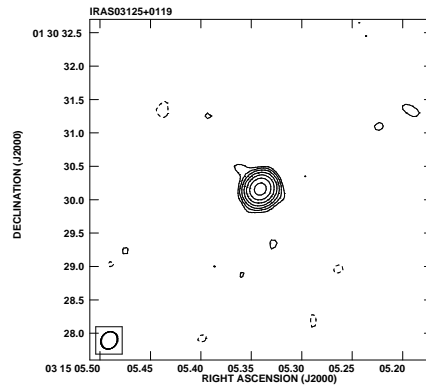
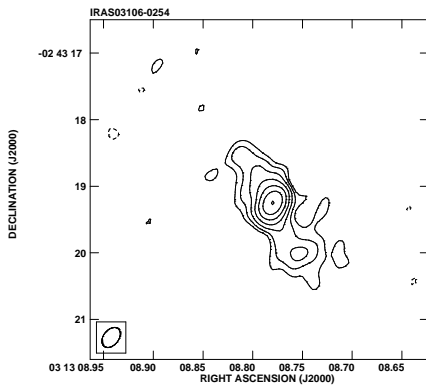
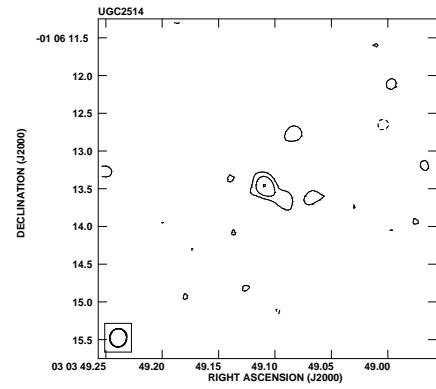
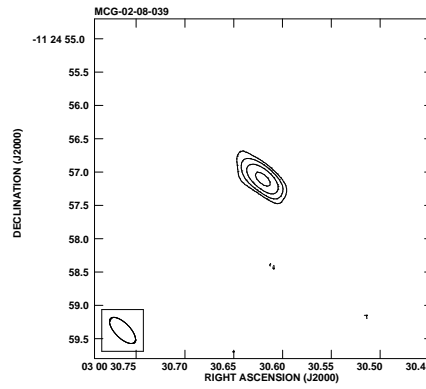
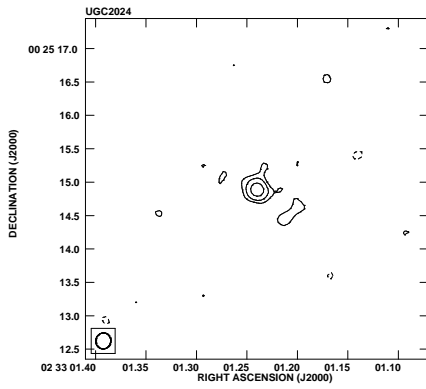
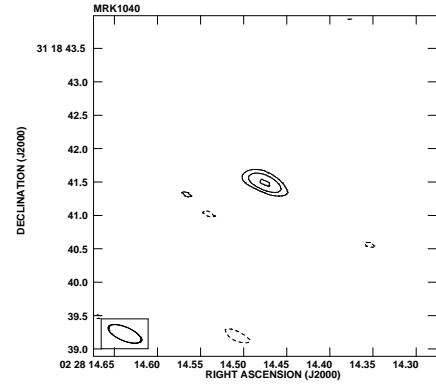
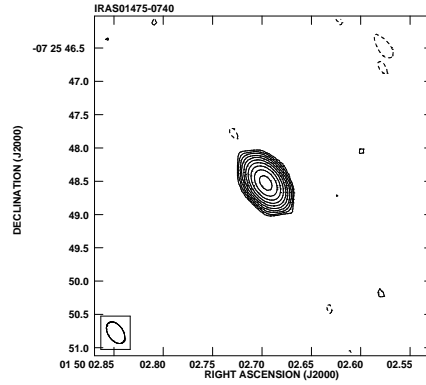
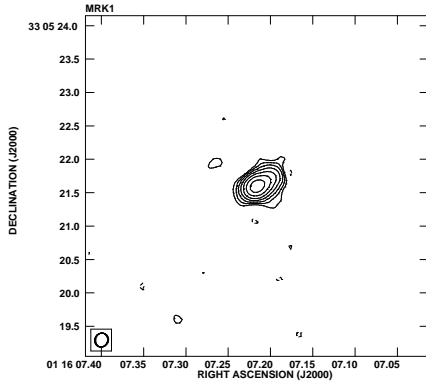
Turner, T. J., George, I. M., Nandra, K. & Mushotzky, R. F. 1997, *ApJS*, 113, 23

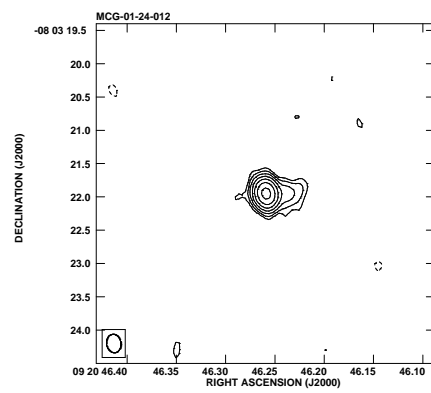
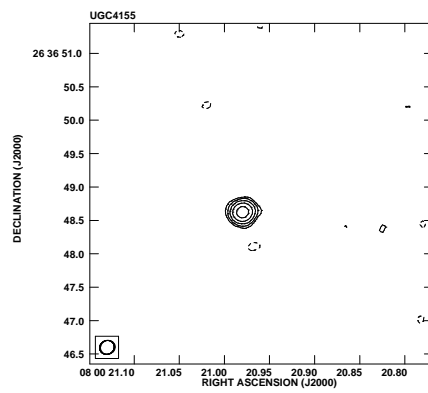
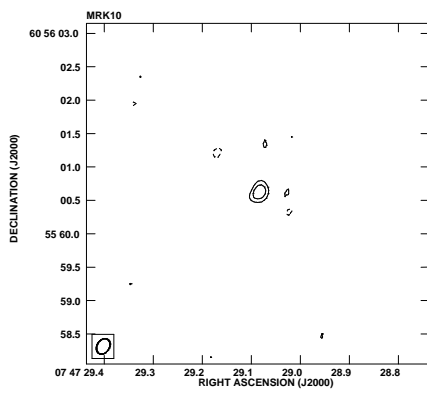
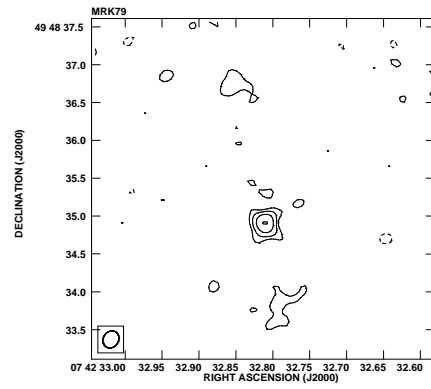
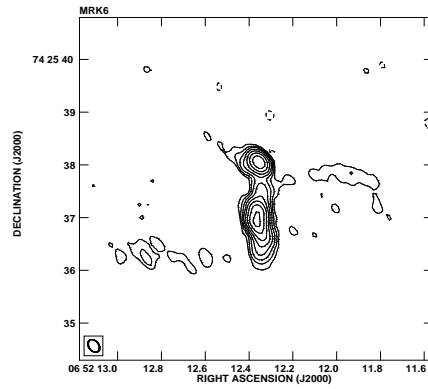
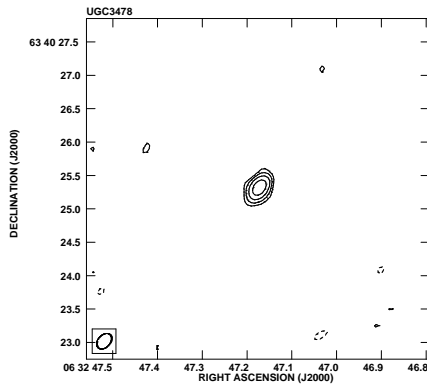
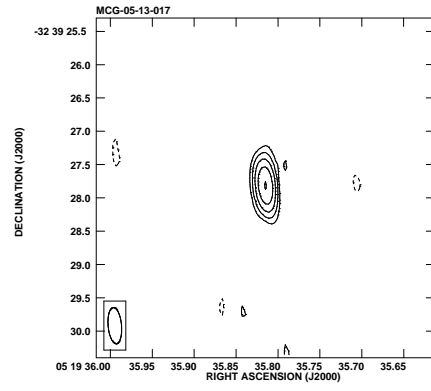
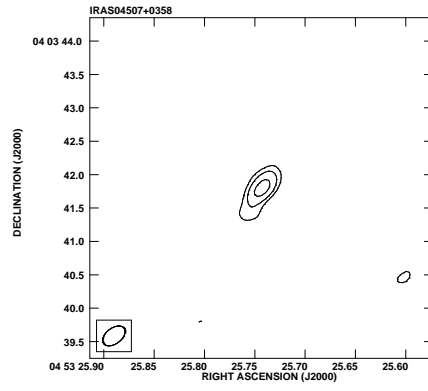
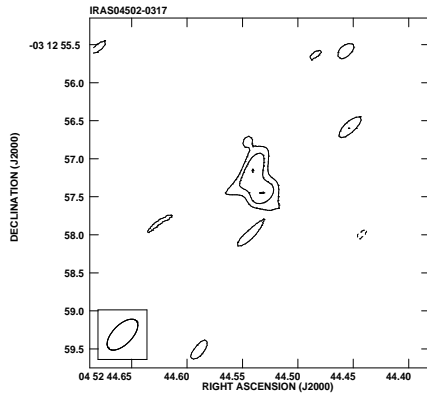
Ulvestad, J.S., & Wilson, A.S. 1984a, *ApJ*, 278, 544

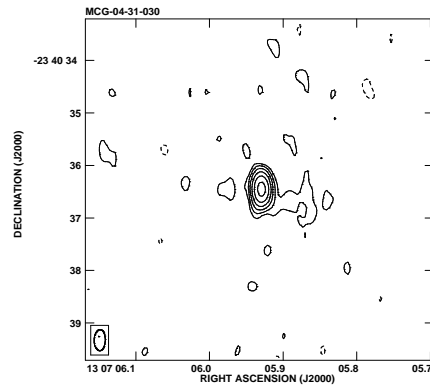
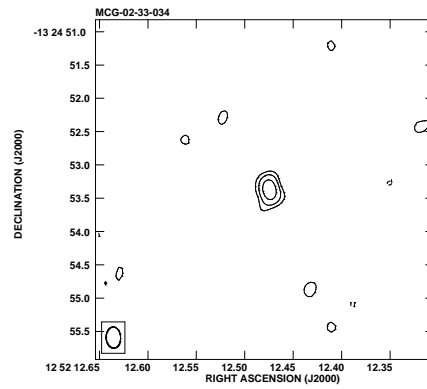
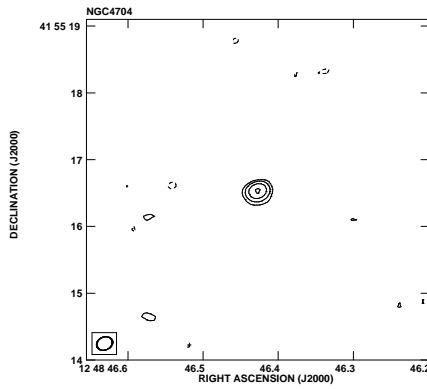
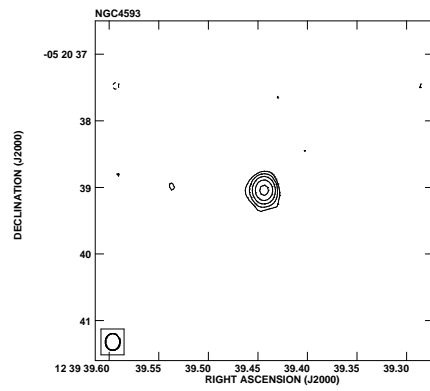
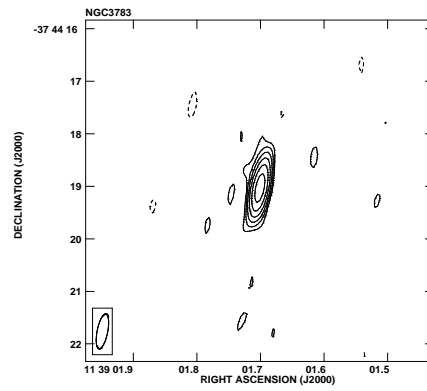
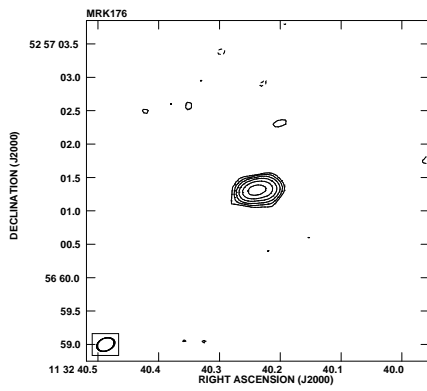
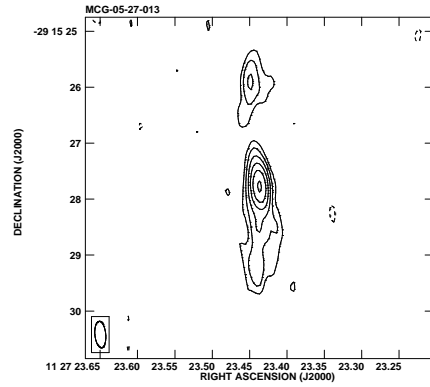
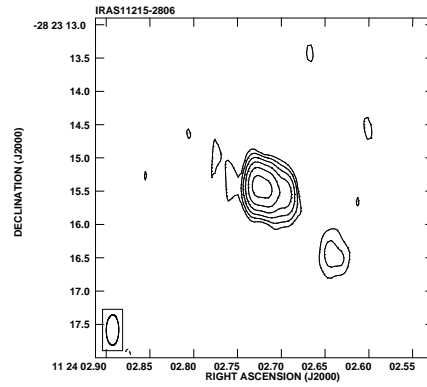
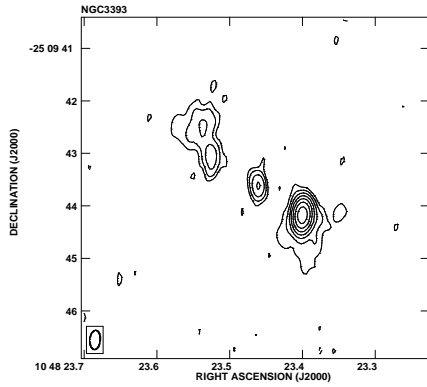
Ulvestad, J.S., & Wilson, A.S. 1984b, *ApJ*, 285, 439

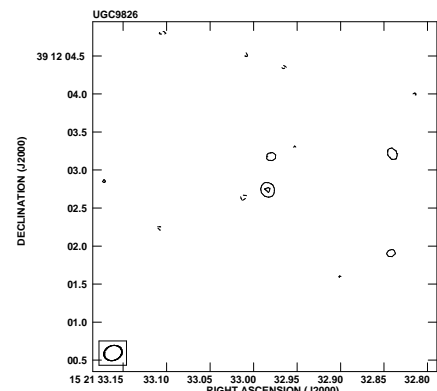
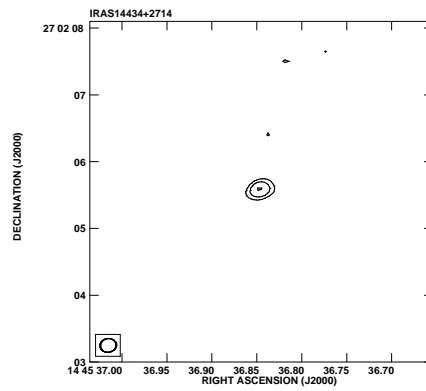
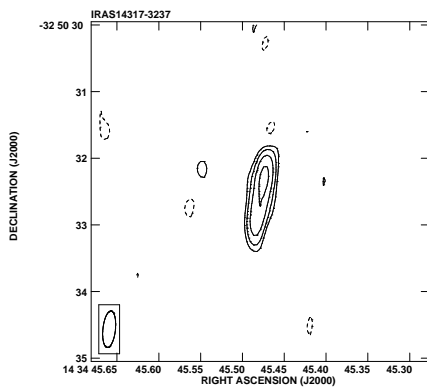
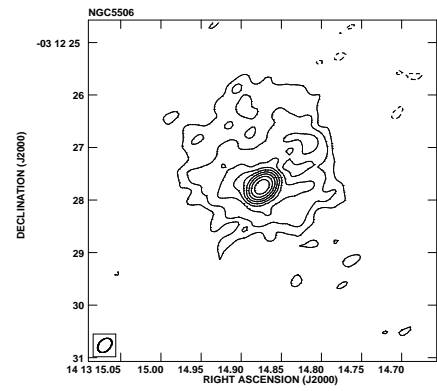
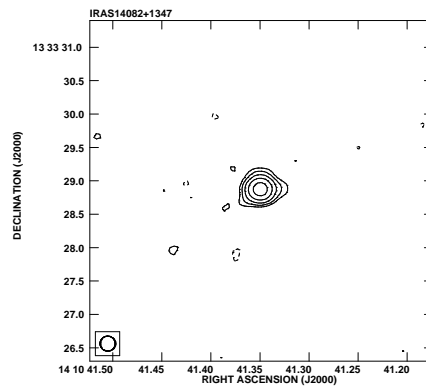
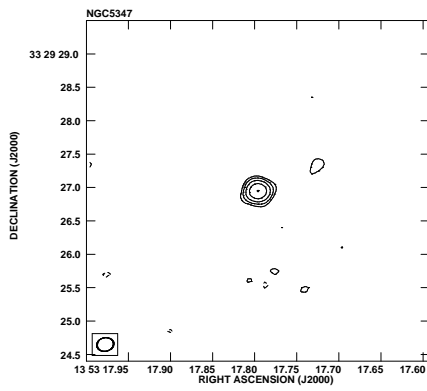
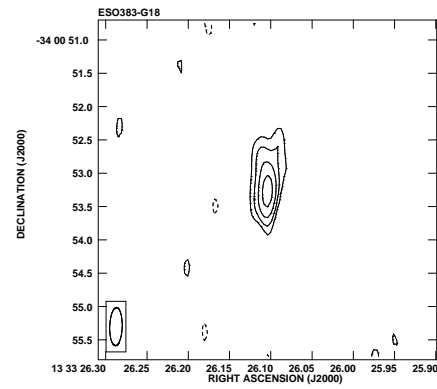
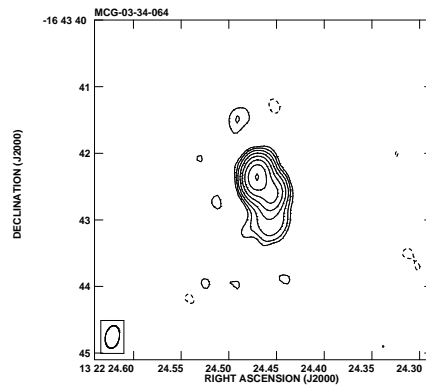
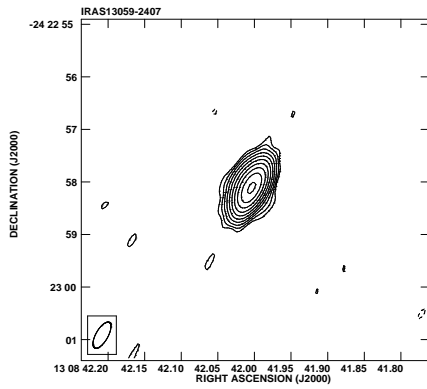
Ulvestad, J.S., & Wilson, A.S. 1986, MNRAS, 218, 711
Ulvestad, J. S. & Wilson, A. S. 1989, ApJ, 343, 659
Veilleux, S., Goodrich, R. W. & Hill, G. J. 1997, ApJ, 477, 631
Wilson, A. S. & Willis, A. G. 1980, ApJ, 240, 429
Xu, C., Baum, S. A., O'Dea, C. & Colbert, E. J. M. 1997, BAAS, 191, 104.05

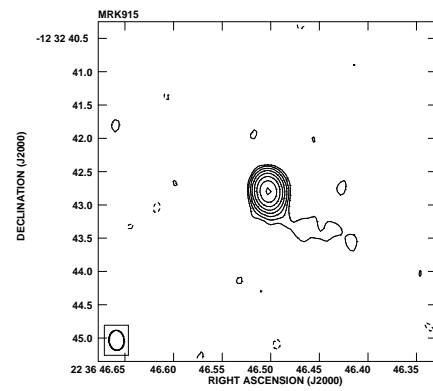
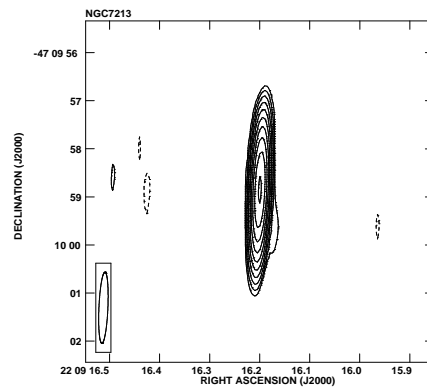
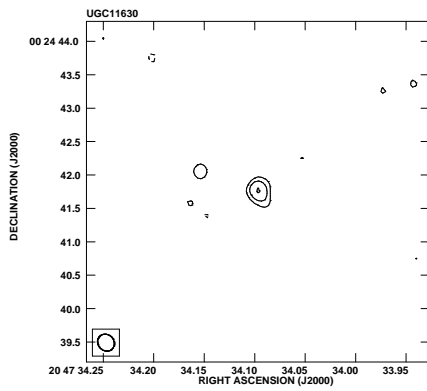
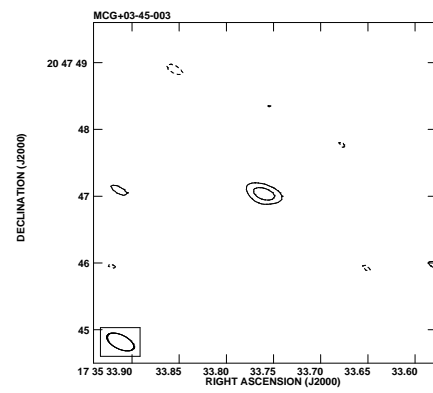
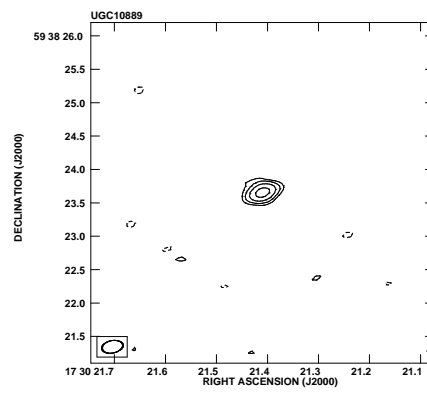
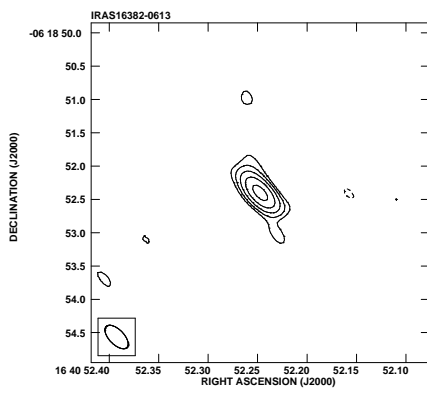
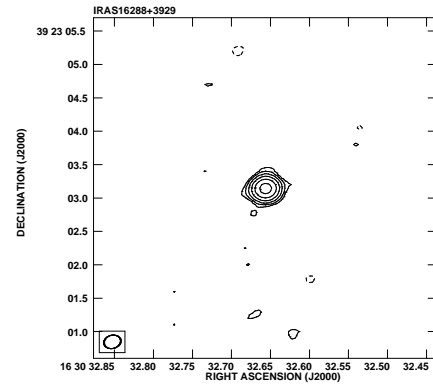
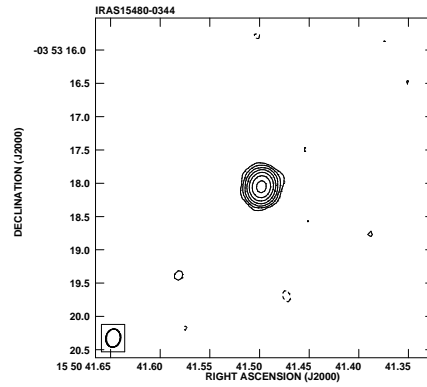
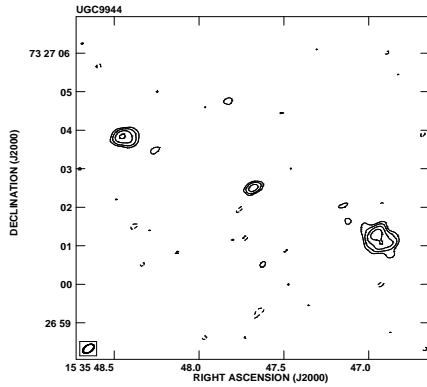
Fig. 1.— Radio continuum 8.46 GHz (3.6cm) contour plots presented following the order given in Table 1. TOL1238-364 is not presented here because it was not detected. The contours start at 3σ above the background level and increase in powers of $\sqrt{2}$ ($3\sigma \times 2^{(n/2)}$, $n=0,1,2,\dots$). We also plot, as a dashed line, the contour plots corresponding to the 3σ level. The lower left corner of each panel shows the shape and size of the restoring beam.











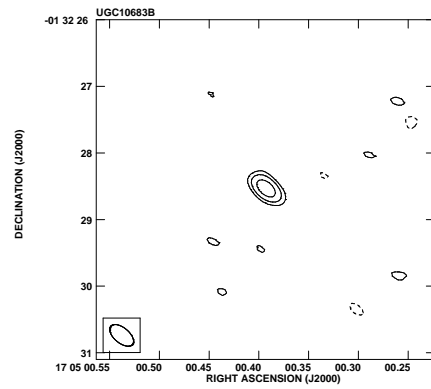
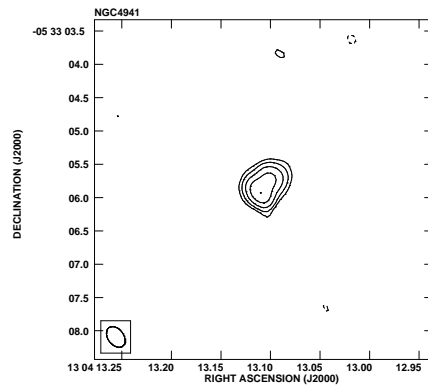
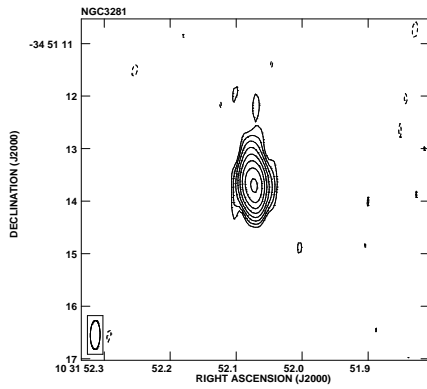
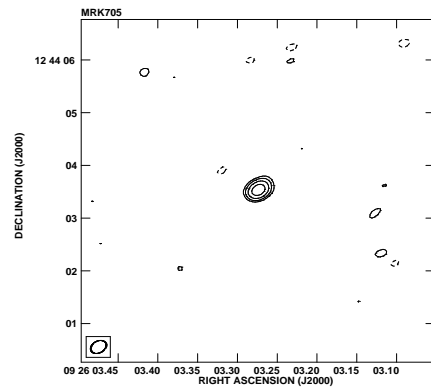
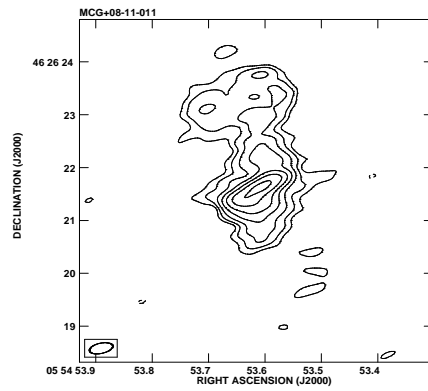
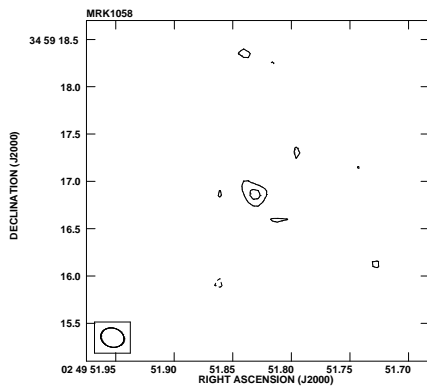
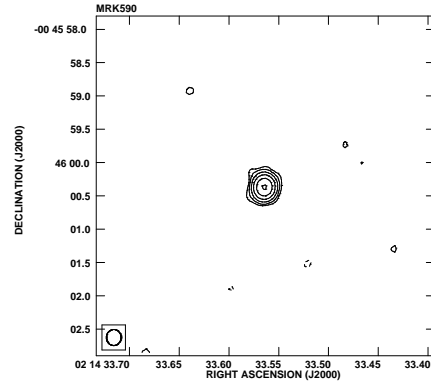
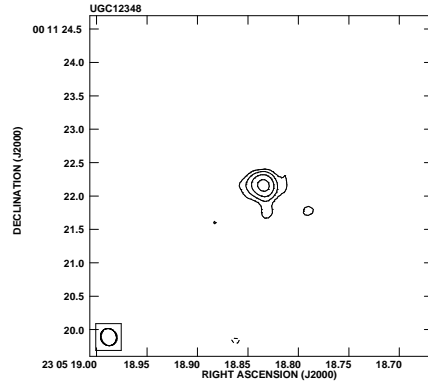
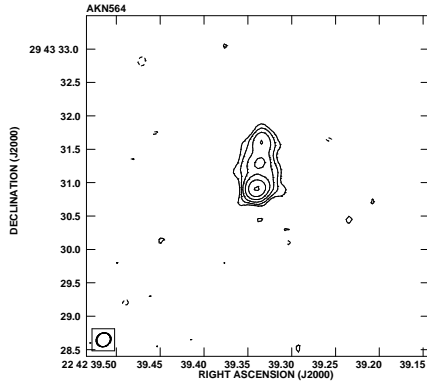


TABLE 1
OBSERVATIONS AND MEASUREMENTS

Number	Name	Type	Date	VLA proposal	Observing Method	$F_{3.6cm}$ (mJy)	σ (μ Jy/B)	PA_{RAD} (degrees)	Size (pc)	Morph.	Ref.
26	MRK 1	2	4-12-98	AA226	CSC...	15.4	30	—	<30	U	
37	IRAS 01475-0740	2	7-15-95	AK394	CS	135.4	62	—	<35	U	1
47	MRK 1040	1	7-15-95	AK394	CS	1.2	89	—	<30	U	1
53	UGC 2024	2	4-12-98	AA226	CSC...	1.2	31	—	<45	U	
67	MCG-02-08-039	2	7-15-95	AK394	CS	2.0	62	—	<55	U	1
68	UGC 2514	1	4-12-98	AA226	CSC...	0.6	31	56	70	L	
75	IRAS 03106-0254	2	5-3-98	AA226	CSC...	11.3	29	37	850	L	
78	IRAS 03125+0119	2	5-3-98	AA226	CSC...	9.1	31	—	<45	U	
141	IRAS 04385-0828	2	7-16-95	AK394	CS	7.6	53	—	<30	U	1
154	IRAS 04502-0317	2	5-3-98	AA226	CSC...	0.5	32	22	110	L	
156	IRAS 04507+0358	2	5-13-98	AA226	CSC...	0.9	33	153	210	S	
174	MCG-05-13-017	1	7-15-95	AK394	CS	2.5	46	—	<25	U	1
203	UGC 3478	1	4-13-98	AA226	CSC...	1.6	32	—	<25	U	
209	MRK 6	1	7-20-95	AK407	CSC...	39.5	24	-3	440	L	1,2
225	MRK 79	1	7-15-95	AK394	CS	2.9	40	11	1260	L	1
227	MRK 10	1	4-13-98	AA226	CSC...	0.3	31	—	<55	U	
233	UGC 4155	1	4-13-98	AA226	CSC...	2.4	31	—	<50	U	
253	MCG-01-24-012	2	4-13-98	AA226	CSC...	9.1	32	89	140	L	
272	NGC 3393	2	11-29-92	AB618	CSC...	13.0	24	56	680	L	
281	IRAS 11215-2806	2	4-13-98	AA226	CSC...	12.0	35	75	400	L	
282	MCG-05-27-013	2	4-13-98	AA226	CSC...	8.4	31	2	1530	L	
283	MRK 176	2	4-13-98	AA226	CSC...	6.3	29	92	140	S	
286	NGC 3783	1	9-1-91	AW278	CSC...	8.0	49	—	<15	U	
301	NGC 4593	1	4-13-98	AA226	CSC...	2.1	31	—	<15	U	
302	TOL 1238-364	2	7-16-95	AK394	CS	—	46	—	—	—	1
306	NGC 4704	2	4-13-98	AA226	CSC...	0.9	31	—	<55	U	
309	MCG-02-33-034	1	7-16-95	AK394	CS	1.3	49	—	<30	U	1
313	MCG-04-31-030	2	7-16-95	AK394	CS	9.4	49	85	480	L	1
314	IRAS 13059-2407	2	3-8-90	AD244	CS	126.0	60	—	<30	U	
317	MCG-03-34-064	2	7-16-95	AK394	CS	49.0	67	39	280	L	1
322	ESO 383-G18	2	4-13-98	AA226	CSC...	2.1	33	178	110	S	
329	NGC 5347	2	4-13-98	AA226	CSC...	1.6	30	—	<15	U	
340	IRAS 14082+1347	2	4-13-98	AA226	CSC...	3.5	30	99	55	S	
341	NGC 5506	2	9-1-91	AW278	CSC...	104.0	43	70 ^a	300	L+D	
349	IRAS 14317-3237	2	4-13-98	AA226	CSC...	2.2	33	169	290	L	
354	IRAS 14434+2714	2	4-13-98	AA226	CSC...	0.4	31	—	<120	U	
369	UGC 9826	1	4-13-98	AA226	CSC...	0.2	31	—	<55	U	
377	UGC 9944	2	4-13-98	AA226	CSC...	6.3	32	67	3430	L	
383	IRAS 15480-0344	2	7-16-95	AK394	CS	11.2	40	—	<60	U	1
409	IRAS 16288+3929	2	4-13-98	AA226	CSC...	5.1	30	—	<60	U	
418	IRAS 16382-0613	2	4-13-98	AA226	CSC...	2.7	32	—	<55	U	
445	UGC 10889	2	4-13-98	AA226	CSC...	1.1	32	—	<55	U	
447	MCG+03-45-003	2	4-13-98	AA226	CSC...	0.3	32	—	<50	U	
510	UGC 11630	2	4-13-98	AA226	CSC...	0.5	31	—	<25	U	
530	NGC 7213	1	7-16-95	AK394	CS	188.0	109	—	<15	U	1
537	MRK 915	1	4-13-98	AA226	CSC...	15.8	32	—	<45	U	
540	AKN 564	1	4-13-98	AA226	CSC...	7.0	27	6	320	L	
549	UGC 12348	2	4-13-98	AA226	CSC...	1.6	31	—	<120	U	
590	MRK 590	1	4-12-98	AA226	CSC...	3.4	30	—	<50	U	
594	MRK 1058	2	5-13-98	AA226	CSC...	0.2	35	—	<35	U	
615	MCG+8-11-11	1	5-13-98	AA226	CSC...	38.4	30	128	1230	L+D	
627	MRK 705	1	3-1-94	AK350	CSC...	2.0	50	—	<55	U	
634	NGC 3281	2	3-24-94	AP276	CSC...	17.0	22	—	<60	U	
665	NGC 4941	2	7-16-95	AK394	CS	4.1	45	-25	15	L	1
703	UGC 10683B	1	4-13-98	AA226	CSC...	0.6	32	—	<60	U	

Col. 1 – Numbers of the galaxies in the de Grijp et al. (1987) catalog.

Col. 2 – Names of the galaxies.

Col. 3 – Activity types.

Col. 4 – Dates when the observation were done.

Col. 5 – VLA proposals from which the data were obtained.

Col. 6 – Method used to observe the source (S) and the phase calibrator (C).

Col. 7 – Integrated 3.6cm flux in mJy.

Col. 8 – 1- σ noise level in μ Jy/Beam.

Col. 9 – Measured position angle of the extended radio emission.

Col. 10 – Size of the radio emitting region (calculated assuming $H_0 = 75 \text{ km s}^{-1} \text{ Mpc}^{-1}$).

Col. 11 – Morphology of the radio emission, U=unresolved, S=slightly resolved, L=Linear, D=diffuse.

Col. 12 – For data obtained from the archive, the reference where it has been published: 1) Thean et al. (2000), 2) Xu et al. (1997).

^aPA_{RAD} obtained from VLBA measurements (Roy et al. 2000).

TABLE 2
POSITIONS AND FLUXES OF INDIVIDUAL COMPONENTS

Name	RA(J2000)	Decl.(J2000)	$F_{3.6cm}$ (mJy)
MRK 1	01 16 07.215	+33 05 21.60	14.8
IRAS 01475-0740	01 50 02.696	-07 25 48.53	135.4
MRK 1040	02 28 14.476	+31 18 41.49	1.1
UGC 2024	02 33 01.240	+00 25 14.89	0.7
MCG-02-08-039	03 00 30.621	-11 24 57.10	2.0
UGC 2514	03 03 49.091	-01 06 13.64	0.2
	03 03 49.109	-01 06 13.47	0.4
IRAS 03106-0254	03 13 08.753	-02 43 20.02	1.0
	03 13 08.780	-02 43 19.27	5.8
	03 13 08.786	-02 43 19.14	4.0
IRAS 03125+0119	03 15 05.341	+01 30 30.16	8.8
IRAS 04385-0828	04 40 54.964	-08 22 22.09	7.5
IRAS 04502-0317	04 52 44.532	-03 12 57.46	0.2
	04 52 44.541	-03 12 57.14	0.2
IRAS 04507+0358	04 53 25.742	+04 03 41.83	0.6
	04 53 25.753	+04 03 41.51	0.2
MCG-05-13-017	05 19 35.815	-32 39 27.81	2.5
UGC 3478	06 32 47.172	+63 40 25.32	1.4
MRK 6	06 52 12.400	+74 25 38.04	10.4
	06 52 12.410	+74 25 37.03	17.0
	06 52 12.400	+74 25 36.81	9.9
MRK 79	07 42 32.785	+49 48 33.85	0.7
	07 42 32.810	+49 48 34.90	1.3
	07 42 32.848	+49 48 36.70	0.9
MRK 10	07 47 29.084	+60 56 00.62	0.3
UGC 4155	08 00 20.980	+26 36 48.62	2.4
MCG-01-24-012	09 20 46.236	-08 03 21.96	0.9
	09 20 46.259	-08 03 21.95	8.0
NGC 3393	10 48 23.380	-25 09 44.07	8.4
	10 48 23.440	-25 09 43.51	0.7
	10 48 23.500	-25 09 42.98	0.8
	10 48 23.520	-25 09 42.37	1.4
IRAS 11215-2806	11 24 02.641	-28 23 16.45	0.7
	11 24 02.696	-28 23 15.54	1.7
	11 24 02.714	-28 23 15.48	4.0
	11 24 02.729	-28 23 15.42	4.4
MCG-05-27-013	11 27 23.437	-29 15 27.78	3.7
	11 27 23.441	-29 15 29.21	0.5
	11 27 23.448	-29 15 25.90	0.5
MRK 176	11 32 40.238	+52 57 01.31	6.3
NGC 3783	11 39 01.670	-37 44 18.85	7.7
NGC 4593	12 39 39.444	-05 20 39.04	2.1
NGC 4704	12 48 46.427	+41 55 16.53	0.8
MCG-02-33-034	12 52 12.475	-13 24 53.38	1.2
MCG-04-31-030	13 07 05.929	-23 40 36.46	5.7
	13 07 05.906	-23 40 36.49	3.5
IRAS 13059-2407	13 08 41.970	-24 22 57.99	126.0
MCG-03-34-064	13 22 24.471	-16 43 42.35	31.6
	13 22 24.456	-16 43 42.61	15.5
ESO 383-G18	13 33 26.105	-34 00 53.25	1.7
NGC 5347	13 53 17.796	+33 29 26.94	1.6
IRAS 14082+1347	14 10 41.350	+13 33 28.87	3.2
NGC 5506	14 13 14.830	-03 12 27.76	73.6
IRAS 14317-3237	14 34 45.474	-32 50 32.29	1.1
	14 34 45.482	-32 50 32.86	0.8
IRAS 14434+2714	14 45 36.846	+27 02 05.58	0.4 ^a
UGC 9826	15 21 32.983	+39 12 02.72	0.2
UGC 9944	15 35 46.919	+73 27 01.07	1.9
	15 35 46.957	+73 27 01.31	1.7
	15 35 47.680	+73 27 02.50	0.6
	15 35 48.443	+73 27 03.82	1.7
IRAS 15480-0344	15 50 41.498	-03 53 18.05	11.2
IRAS 16288+3929	16 30 32.656	+39 23 03.14	4.8
IRAS 16382-0613	16 40 52.248	-06 18 52.40	2.1
UGC 10889	17 30 21.410	+59 38 23.66	1.1
MCG+03-45-003	17 35 33.761	+20 47 47.04	0.3
UGC 11630	20 47 34.096	+00 24 41.76	0.4
NGC 7213	22 09 16.200	-47 09 58.85	187.9
MRK 915	22 36 46.503	-12 32 42.80	14.5
	22 36 46.467	-12 32 43.36	0.2

TABLE 2—*Continued*

Name	RA(J2000)	Decl.(J2000)	$F_{3.6cm}$ (mJy)
AKN 564	22 42 39.334	+29 43 31.59	0.9
	22 42 39.337	+29 43 31.24	3.0
	22 42 39.340	+29 43 30.91	3.1
UGC 12348	23 05 18.836	+00 11 22.16	1.1
MRK 590	02 14 33.564	-00 46 00.37	3.2
MRK 1058	02 49 51.842	+34 59 16.90	0.2
MCG +8-11-11	05 54 53.613	+46 26 21.57	24.4 ^b
MRK 705	09 26 03.260	+12 44 03.46	2.0
NGC 3281	10 31 52.050	-34 51 13.55	17.0
NGC 4941	13 04 13.110	-05 33 05.96	1.2
	13 04 13.104	-05 33 05.77	2.8
UGC 10683B	17 05 00.393	-01 32 28.53	0.6

^aThere is a second radio source 21'' N of IRAS14434+2714, probably related to a fainter background galaxy, which can be seen on the HST archival image. This source can be decomposed in two components at RA(J2000)=14:45:36.909, DEC(J2000)=+27:02:27.11 and RA(J2000)=14:45:36.915, DEC(J2000)=+27:02:27.30 with 3.6cm fluxes 0.9mJy and 7.5mJy, respectively.

^bCore component only.